

Meteorological analysis of the tornado in Ciudad Acuña, Coahuila State, Mexico, on May 25, 2015

José F. León-Cruz¹ · Noel Carbajal¹ · Luis F. Pineda-Martínez²

Received: 2 August 2016 / Accepted: 15 June 2017 / Published online: 22 June 2017
© Springer Science+Business Media B.V. 2017

Abstract Extreme meteorological conditions favor the development of severe storms and tornadoes that may have largely impacts on the population despite its relatively short life. Tornadoic severe storms have been documented around the World. In Mexico (MEX), the study of the occurrence of tornadoes and severe storms is relatively new. In this research, we have selected an event of severe tornadoic storm in Ciudad Acuña, Mexico. The storm was driven by a frontal system moving southward from USA converging with a warmer moist air flux from the Gulf of Mexico. The tornado strikes on the Northeast of Mexico, in Coahuila State, on May 25, 2015. Imagery of infrared channel from GOES 13 satellite and the presence of a hook echo in radar data of May 25, 2015, indicate a supercell structure. The maximum values of radial velocity were about -20 and 15 m s^{-1} . In this study, the WRF model was used in order to simulate the mesoscale meteorological conditions of the tornado. Model simulations capture atmospheric features observed in Doppler radar. The simulated storm-relative helicity values were between 400 and $500 \text{ m}^2 \text{ s}^{-2}$. The simulated convective available potential energy values were of 3000 J kg^{-1} . These values were higher than values for convective storms, located over the region of Ciudad Acuña in Mexico and Del Rio in USA. The supercell was a result of high humidity and temperature gradients, conditioned by frontal activity and moisture flux intensifications from the Gulf of Mexico.

Keywords Tornado event · Mesoscale modeling · Severe storm

✉ Luis F. Pineda-Martínez
lpineda@uaz.edu.mx

¹ División de Geociencias Aplicadas, Instituto Potosino de Investigación Científica y Tecnológica, 78216 San Luis Potosí, Mexico

² Unidad de Ciencias de la Tierra, Universidad Autónoma de Zacatecas, 98600 Zacatecas, Mexico

1 Introduction

Severe storms and tornadoes originate and evolve in extreme meteorological conditions, with large impacts on the population despite its relatively short life. Severe thunderstorms and tornadoes are closely related. The tornadoes can be classified in two types: first those that derived from mesocyclone circulation, with an isolated supercell, a supercell in a line of thunderstorms or a mini supercell with a small mesocyclone as a parent storm. The second type is not associated with a mesocirculation and is generally a small and weak vortex formed along a stationary and or slowly moving wind shift line (Davies-Jones et al. 2001). In general, tornadoes present wind speeds between 20 and 140 m s⁻¹, and they are classified with the Fujita scale (Fujita 1971). Its diameter is usually 200 m or more and its life lasts from just a few seconds to more than an hour (Bluestein 2013). Although the major number of reported tornadoes is in USA, an average of over 1000 each year (NCDC 2016), tornadoes have been observed and documented in all the continents except Antarctica (Goliger and Milford 1998).

Brooks et al. (2003a) determined a temporal and spatial distribution of environmental conditions associated with significant severe thunderstorms and discriminated between tornadic and non-tornadic thunderstorms in eastern USA. By applying those relationships for the entire globe, it was able to found values of frequency of favorable conditions for significant severe thunderstorms. Those results depict the greatest frequency of tornadic storms over the central plains of USA, with lesser areas in southern Brazil and northern Argentina (Brooks et al. 2003a).

Although tornadoes are more studied and documented in USA, several studies have been realized in different parts of the world as Spain (Mateo et al. 2009), Italy (Gianfreda et al. 2005), Greece (Matsangouras et al. 2011, 2014b), Colombia (Ortiz-Royero and Rosales 2012), India (Litta et al. 2012), Bangladesh (Akter and Ishikawa 2014), and China (Yao et al. 2015). In many cases, the lack of meteorological remote sensing data such as data from radars and soundings led to the application of numerical models. Numerical models have been implemented as a useful tool for determining meteorological conditions during tornadoes and severe storms.

In Mexico, the occurrence of tornadoes and severe tornadic storms has been described since the colonial time (Fuentes 2010). However, the study of tornadoes is relatively new, and the first climatology data of tornadoes have recently published by Medrano and García (2014).

In this study, the selected tornado occurred in Ciudad Acuña, Mexico on May 25, 2015, that according to our data is classified as the most destructive over Mexican territory, causing a significant social and economic impact. Our objectives were: Firstly, it was to analyse the atmospheric conditions that favor the development of tornado and secondly to investigate the ability of The Weather Research and Forecasting Model-Advanced Research (WRF-ARW) model to simulate this event by examine several atmospheric parameters that favor tornadogenesis. The WRF-ARW model was used to simulate the meteorology and mesoscale precedent conditions of the tornado. The event was also selected for proving the ability of mesoscale numerical model in characterizing the weather features associated with tornadic storms. Additionally, imageries from the Geostationary Operational Environmental Satellite (GOES) 13, Next Generation Weather Radar (NEX-RAD) data, and meteorological reports of the National Weather Service of Mexico (SMN) were used.

2 Data and methodology

2.1 Tornado case

The severe storm occurred near the border USA–MEX in Ciudad Acuña, Coahuila, Mexico (Fig. 1a). The tornado occurred on May 25, 2015, and according to household information, the event took place close to 5:50 (10:50 UTC) and ended at 06:10 local time (11:10 UTC). A track of 1.83 km in southwest–northeast direction was calculated (Fig. 1c). Civil Protection Coordinator of Mexico classified this tornado as F3 on Fujita Scale, with calculated wind speed between 70 and 92 m s⁻¹.

The tornado caused 14 fatalities, 290 people injured and several material damages. The Mexican government enabled 8 shelters and the region was declared as an emergency and disaster zone. The estimation of the SMN of the Ciudad Acuña tornado was EF3 in the Enhanced Fujita scale, based in the damages and the wind velocities (SMN 2015). The total damage was calculated in 250 Mexican million pesos only for infrastructure and residential rehabilitation.

2.2 Numerical model settings

The WRF model is a numerical weather prediction and atmospheric simulation system designed for both research and operational applications (Skamarock et al. 2008). The development of the WRF is a collaborative project among institutions as the National Center for Atmospheric Research (NCAR), the National Oceanic and Atmospheric Administration's (NOAA), the Department of Defense's Air Force Weather Agency (AFWA). The WRF-ARW modeling system is suitable for use in abroad range of applications, as idealized simulations, parameterization research, data assimilation research, real-time NWP or hurricane research (Wang et al. 2007). In this study the WRF-ARW version 3.6.1 model was used in order to simulate the meteorological conditions that favor the development of tornado in Ciudad Acuña, Coahuila, Mexico on May 25, 2015. One

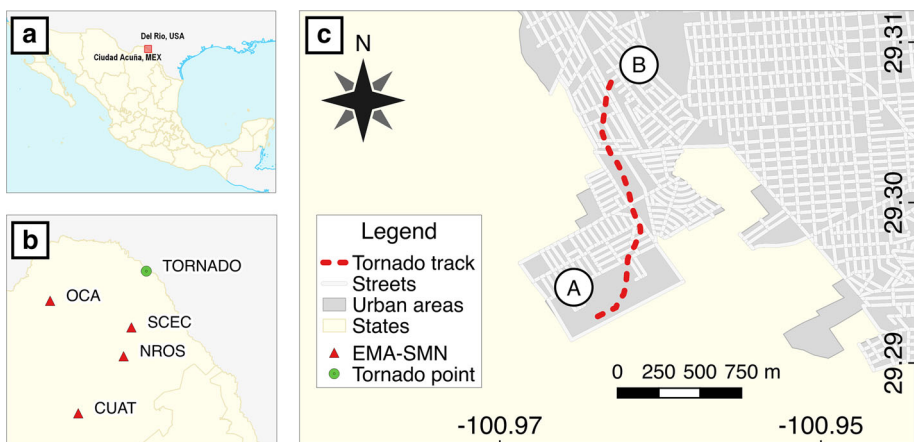
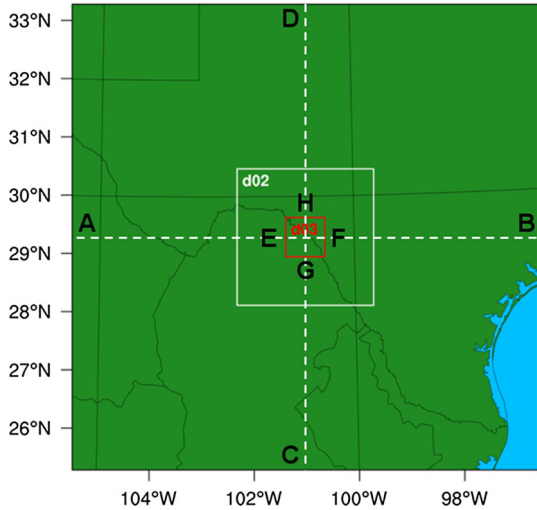


Fig. 1 a Location maps of the tornado on May 25, 2015. b Location of the validation meteorological stations: Ocampo (OCA), Santa Cecilia (SCEC), Nueva Rosita (NROS) and Cuatro Ciénegas (CUAT). c Map of the track of the tornado over the urban area of Ciudad Acuña, Mexico. The transect A–B designate the approximate starting and endpoint

Fig. 2 WRF Domain configuration for tornado case. Dashed lines indicate cross-section locations



mother domain with 2 nested domains were used, all of them centered on 29.29° LAT, -100.96° LON (Fig. 2). The domains configurations were a mother domain of 100×100 grid points with a resolution of 9 km (d1). Domain d2 (d3) characterized by 88×88 (76×76) grid points and a resolution of 3 (1) km. The model was initialized with final analysis data from National Centers for Environmental Prediction (NCEP) Final Analysis (FNL) at 6-h temporal resolution (NCEP 2015). The model simulation was initiated at May 24, 2015, at 00:00 UTC and finished on May 26, 2015, at 00:00 UTC. The models outputs were obtained every 10 min for domain d1, 180 min for nest domain d2, and 10 min for the domain d3 (Fig. 2).

The model physics configuration included the WRF Single-Moment 3-class scheme for microphysics (Hong et al. 2004), Rapid Radiative Transfer Model scheme (RRTM scheme) for Longwave Radiation (Mlawer et al. 1997), Dudhia scheme for Shortwave Radiation (Dudhia 1989), Kain–Fritsch scheme for Cumulus Parameterization (Kain 2004), and Yonsei University scheme (YSU scheme) for Planetary Boundary Layer (Hong et al. 2006).

3 Synoptic analyses and remote sensing

3.1 Synoptic scale analysis

Figure 3a, b illustrates synoptic upper air analysis of 500 and 850 hPa pressure levels on May 24 and 25, 2015, at 12:00 UTC, respectively. The frontal system is driven by a cold air mass moving southward from high latitudes at middle atmospheric levels at 500 hPa (Fig. 3a). This air mass converges with a warmer moist air flux from the Gulf of Mexico at low levels generating a high vertical winds shear in the front edge (Fig. 3b). Those air masses with different converging properties have been described as key elements in generating severe storms with high potential of tornadogenesis (Markowski and Richardson 2009). The cold air mass traveling from the mountain region in the northwest of USA generates high steep lapse rates, associated with formation of tornadic supercells (Doswell and Burgess 1993; Markowski and Richardson 2009).

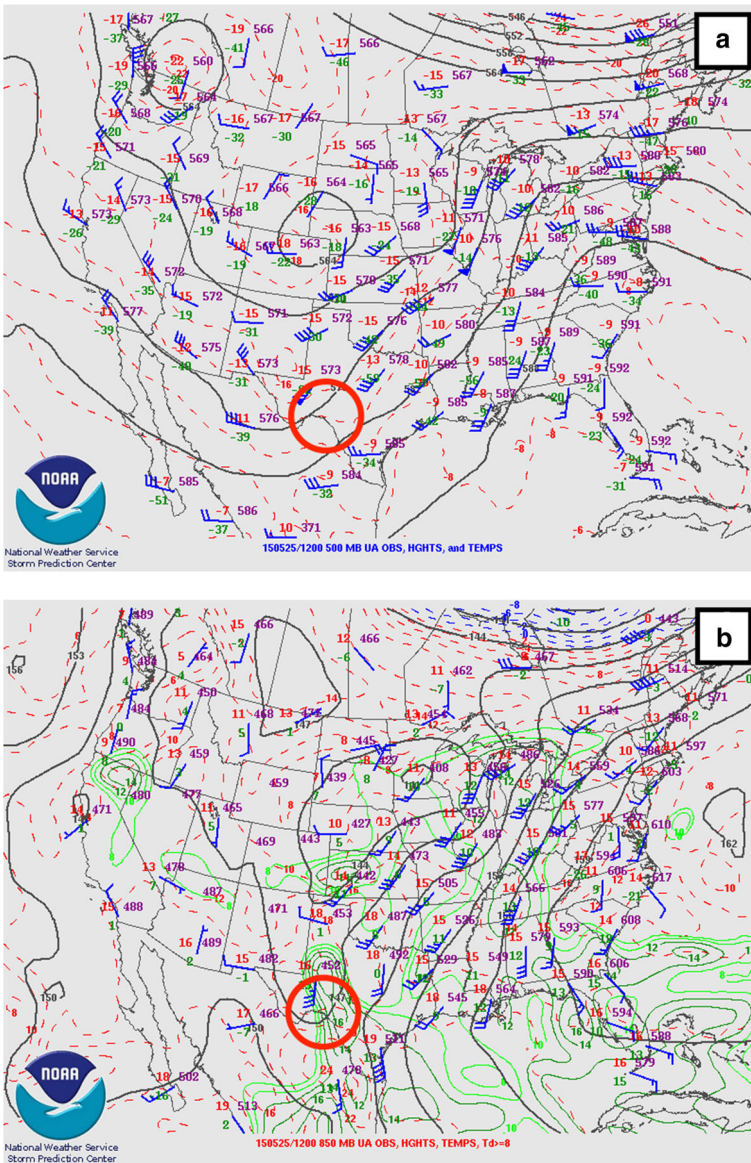


Fig. 3 Synoptic weather maps (station data and analysis) at **a** 500 hPa and **b** 850 hPa on May 25, 2015, at 12:00 UTC. *Dashed lines* indicates temperature and *solid lines* indicates height. *Source*: NCAR (2015). The *red circle* indicates the tornado position

During the storm of May 25, many of the described factors were determinant for convective storms and threat of tornadoes. Severe storm and tornadic activity follow a seasonal pattern as it has been described by Brooks et al. (2003b). Thus, this climatology of tornadoes indicates a maximum threat of tornadoes pattern. According to Brooks et al. (2003b), the formation of tornadoes in southern Texas shows a maximum early in the season of severe convective storms in May. This could be associated with circulation

patterns of cold air masses in late cold period and an intensification of moist fluxes from the Gulf of Mexico in early warm period (Fig. 3b).

This seasonal pattern of maximum threat moves toward northeast just to the Tornado Alley (central plain region over southern USA), where the maximum occurrence is during the months of June and July (Doswell and Burgess 1993; Brooks et al. 2003b). The intensification of the severe storms season largely depends of the increase in convective processes because of thermal contrasts of air masses that dominate in the plains in central USA (Doswell and Burgess 1993). Although the mechanisms of supercell tornadic storms formation are similar and almost well-identified patterns (Rasmussen et al. 1994), many of these processes respond in different ways depending on the properties of air parcels, thermal conditions, and moisture content. Specifically, it is necessary a high gradient in temperature and moisture content for inducing high vertical wind shear and high horizontal vorticity (Rasmussen et al. 1994).

3.2 Satellite imagery

Imagery in the infrared channel, from GOES 13 satellite from 08:45 to 11:45 UTC in a 1-h step on May 25, 2015, is shown in Fig. 4. Two convective systems are observed over Chihuahua and Coahuila moving northeast. The system, located on the southern region, caused the tornado in Ciudad Acuña, Coahuila (Fig. 4a). The convective clouds started to develop near to 08:15 UTC (not shown), approximately 180 km from Ciudad Acuña. At 08:45 UTC, those systems were extended in northwest–southeast direction. One central core and the beginning of the other are visible in Fig. 4a. At 09:45 UTC, two storm compact cores were situated over Ciudad Acuña (Fig. 4b). Approximately, at the time of tornado touchdown (10:45 UTC), the central storm core was located over Ciudad Acuña, and the cloud system is well defined in the Fig. 4c. Its extension was approximately of 150 km × 110 km, and the cloud top temperature was $-63\text{ }^{\circ}\text{C}$ (210 K), an indicator of very high cloud tops, nearly of 13 km. The estimated minimum temperature was approximately $-87\text{ }^{\circ}\text{C}$ (186 K). High clouds with very low temperatures (lower than $-70\text{ }^{\circ}\text{C}$) are associated with strong updrafts and severe storms (Mateo et al. 2009; Weisz et al. 2015; Matsangouras et al. 2016).

The system continued in southwest–northeast direction, crossing USA–MEX border as a mesocyclone at 11:55 UTC (Fig. 4d). According with the Storm Prediction Center in USA (SPC 2015), on May 25, 2015, there were 281 severe storm reports (26 tornadoes; 188 wind; 67 hail), most of them in Texas (not shown). However, the tornado of Ciudad Acuña in Mexico was the only event that was reported by the SMN.

3.3 Doppler weather radar (DWR) imagery

The observations of DWR have been used worldwide to determinate the characteristics of severe storms, including tornadoes. Several studies were performed using the DWR as a very effective tool for the detection of tornado parameters, not only in USA, but also in different parts of the world. In this sense, Ryzhkov et al. (2005) found that unusual polarimetric debris signatures observed in tornadic storms can be used in the detection of strong tornadoes. Those criteria were the presence of hook echo, critical values of differential reflectivity, and high values of radar reflectivity.

Figure 5 shows NEXRAD II images. The data were obtained from the National Centers for Environmental Information (NCEI) and National Oceanic and Atmospheric Administration (NOAA) at three different times of radar reflectivity and radial velocity. The storm

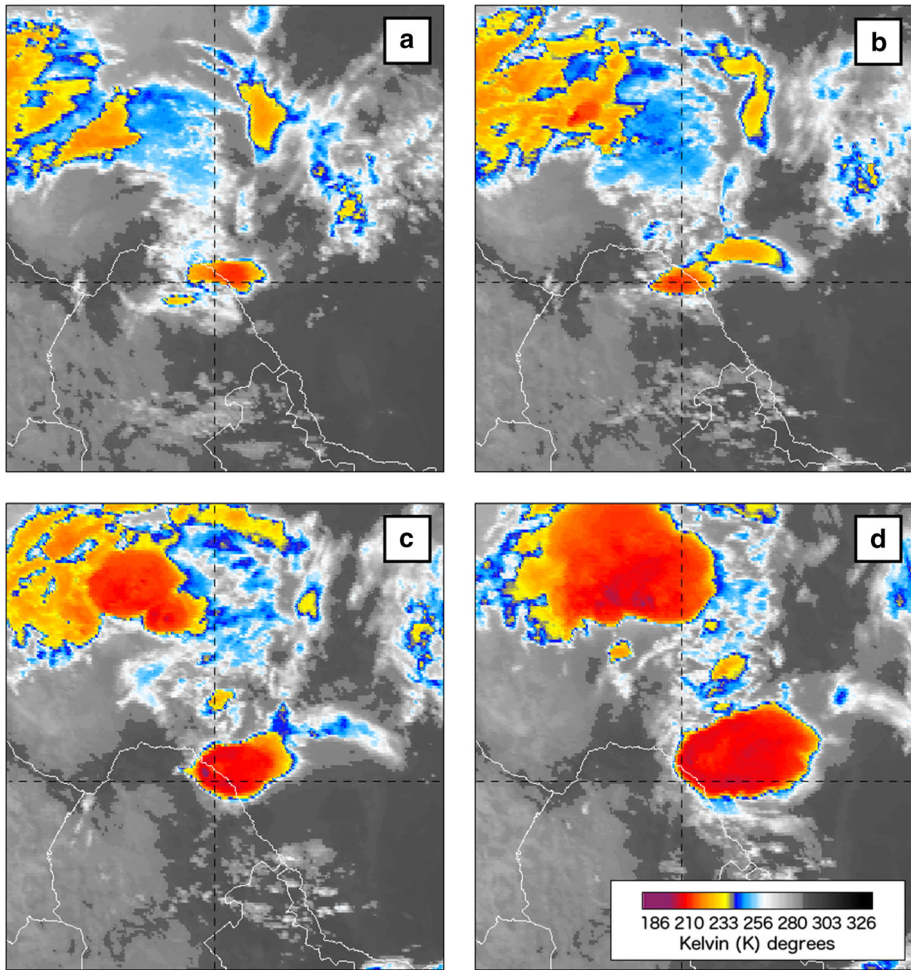


Fig. 4 GOES 13 satellite imageries on infrared band (brightness temperature in Kelvin) from **a** 08:45 UTC, **b** 09:45 UTC, **c** 10:45 UTC and **d** 11:45 UTC on May 25, 2015. The *lines intersection* indicates de location of Ciudad Acuña, Coahuila

started approximately at 08:15 UTC (not shown). The convective storm continued moving in the northeast direction, and at 09:50 UTC had an extension of ~ 100 km with a maximum reflectivity core of 64 dBZ (Fig. 5a). In Fig. 5b, it is possible to observe the structure of a supercell storm at 10:50 UTC, at the time of the occurrence of the tornado. The presence of a hook echo is also clearly observed. In the region of the hook echo, the maximum reflectivity was 64 dBZ, indicating a high damage potential (Ryzhkov et al. 2005; Simeonov et al. 2013). The radial velocity is shown in Fig. 5b; the maximum values recorded were about -20 and 15 m s^{-1} .

At 11:50 UTC, the supercell continued moving northeast through Texas (Fig. 5c) with an area of about 45 km^2 and a maximum reflectivity of 55 dBZ (indicating a strong thunderstorm yet). The radar reflectivity plot (Fig. 5c) shows a bifurcation of the system,

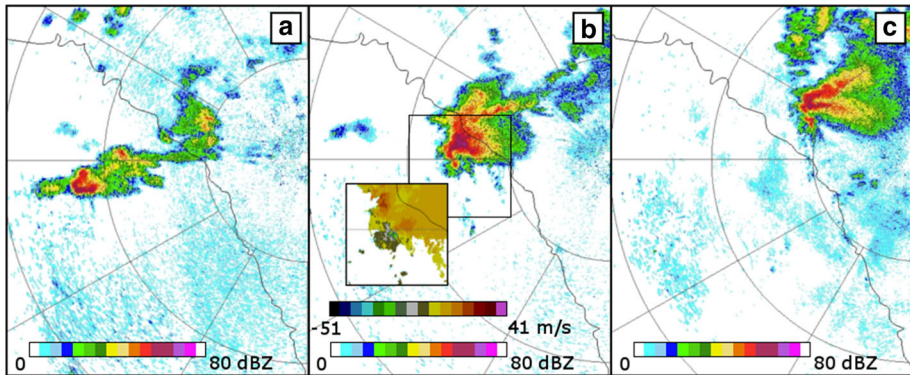


Fig. 5 Radar reflectivity (dBZ) from the WSR-88D radar in Laughlin Air Force Base, Texas at: 9:50 (a), 10:50 (b) and 11:50 (c) UTC. All data are at an elevation of 0.5°. Radial velocity is shown in the second panel, approximately at the time of the tornado (10:50 UTC)

which is an evidence of the V-notch signature of a strong high supercell (Westbrook and Clark 2013).

4 Results and discussion

4.1 Evaluation of model simulations

The WRF outputs were compared against observed parameters to evaluate the model performance. The observed data were obtained from four automatized meteorological station of SMN around Ciudad Acuña (See Fig. 1b).

Figure 6 presents the scatter plots between observed and calculated data for temperature, relative humidity, and pressure at the stations Santa Cecilia (SCEC) and Nueva Rosita (NROS). Additionally, root-mean-square error (RMSE) and BIAS were calculated, and the results are depicted in Table 1.

4.2 Surface modeled features

4.2.1 Temperature, pressure, and humidity

The model results at 10:00 UTC and 11:00 UTC for domain d1 of specific humidity and wind vectors are shown in Fig. 7a, b. It can be seen the strong gradient of moisture content at 11:00 UTC (Fig. 7a) and at 12:00 UTC (Fig. 7b). In the area where the tornado occurred, a contrast in specific humidity values and in wind gradients can be observed.

The cold dry mass air propagating southward converges with a warm moist air mass from the Gulf of Mexico (Fig. 8) with a temperature gradient between the northwest and southeast regions of about 10 °C. In Fig. 8a, a big zone with relative humidity values of more than 90%, i.e., near saturation point of water vapor is observed. These conditions induce strong convective activity and severe storms (Pineda-Martinez and Carbajal 2009; Litta et al. 2012). In the studied case, that weather conditions and a strong wind shear just on the front leading edge caused a supercell storm with high potential of tornado genesis (SPC 2015). Tornadoes categorized as EF2 and higher commonly are generated in

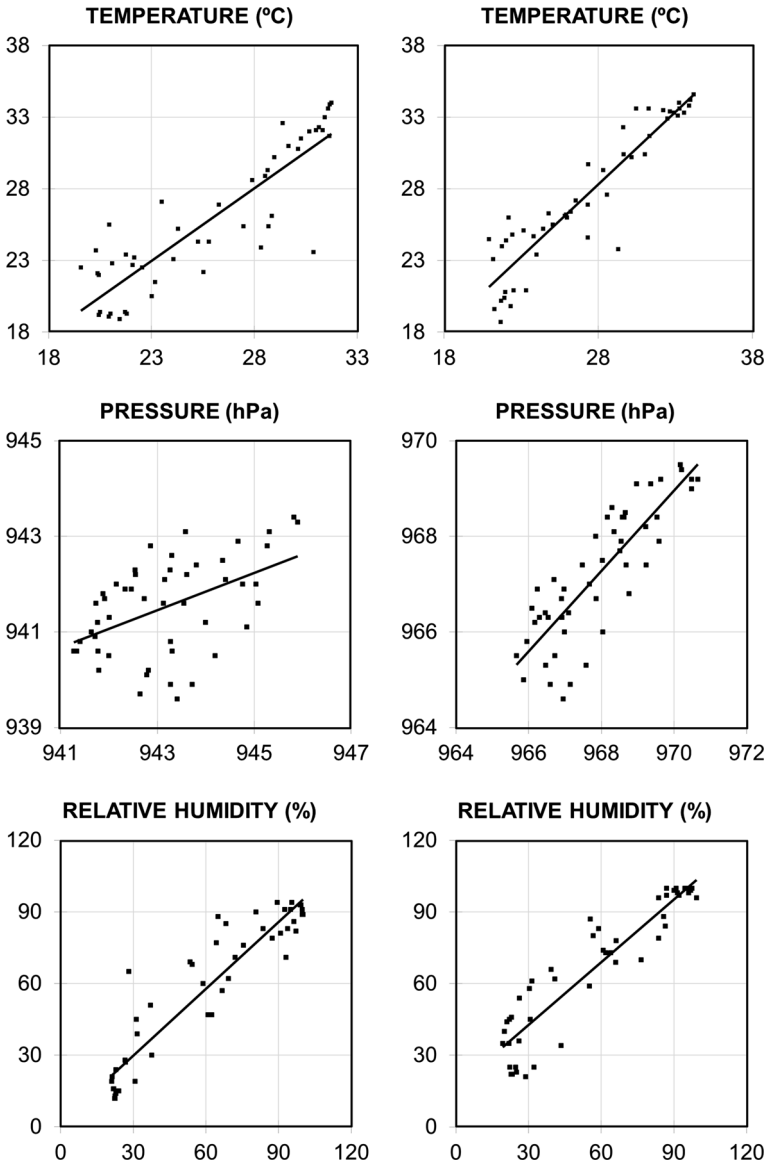
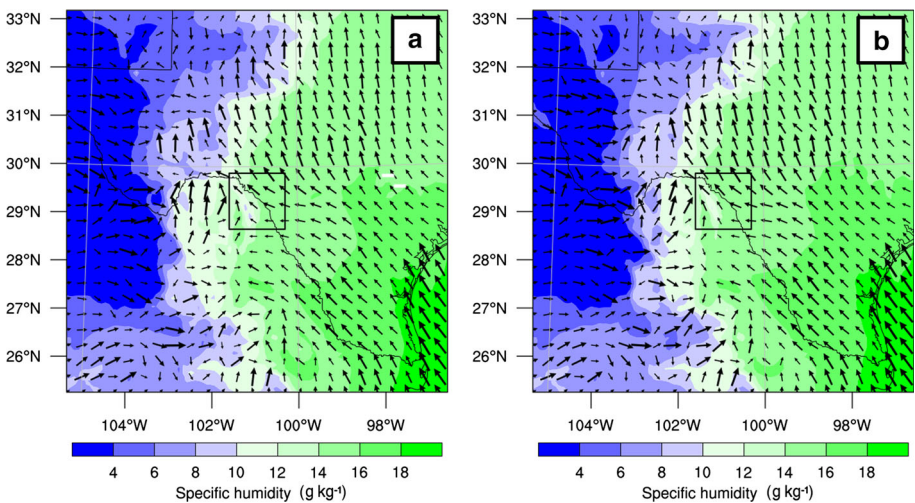


Fig. 6 Modeled and observed 1-h variations of temperature, relative humidity and pressure in NROS (*right*) and SCEC (*left*) meteorological stations

supercell storms (Markowski and Richardson 2009). Those storms are characterized by a rotating updraft due to the horizontal gradient winds and strong vertical wind shear (Doswell and Burgess 1993; Markowski and Richardson 2009). Those unstable atmospheric conditions with strong updrafts due to forced convection produced buoyant air masses, causing an acceleration of the air mass upward. From the model simulation, it is observed that the dry line formation is south–north oriented (Fig. 8a), coinciding with the storm observed in Doppler radar. The vertical turbulent moist fluxes, produced by

Table 1 Parameters calculated

Parameters/ station	RMSE			BIAS		
	Temperature (°C)	Relative humidity (%)	Pressure (hPa)	Temperature	Relative humidity	Pressure
NROS	1.81	13.99	1.06	−0.31	−8.91	0.69
CUAT	3.20	20.06	1.92	−1.37	8.86	1.53
OCA	1.25	17.98	3.74	−0.07	10.79	3.35
SCEC	2.29	11.86	2.04	−0.01	2.51	1.68

**Fig. 7** Model simulated specific humidity (g kg^{-1}) and wind vectors for domain d1 at 10:00 UTC (a) and at 11:00 UTC (b) of May 25, 2015

convergences and divergences motions, caused a high moist concentration near the leading edge of the front (Fig. 9). This can be observed in the west–east cross section A–B (see Fig. 2), where relative humidity values reveal a front-like pattern (Fig. 9a). On the contrary, the moist concentration is very high along the cross section C–D (Fig. 9b).

4.2.2 Thunderstorm-associated winds

The event of Ciudad Acuña was cataloged as a supercell tornado as EF2 (SPC 2015), although during its life time the tornadoes can reach all the spectrum of intensity from EF0 through EF5 (Agee and Jones 2009). The recorded wind speed in surrounding sites reaches 16 m s^{-1} and gusts of 26 m s^{-1} (SMN 2015). Nevertheless, the damage scenery suggests wind speeds much more higher in main tornado vortex or the funnel area (SPC 2015). The modeled wind components show maximum velocities between 8 and 10 m s^{-1} on surface at the time the tornado touchdown in Ciudad Acuña, indicating obviously an underestimated value (Fig. 10). A zone with large velocity values is observed on the northern side of the region where the tornado occurred. It coincides with the trajectory followed by the storm system.

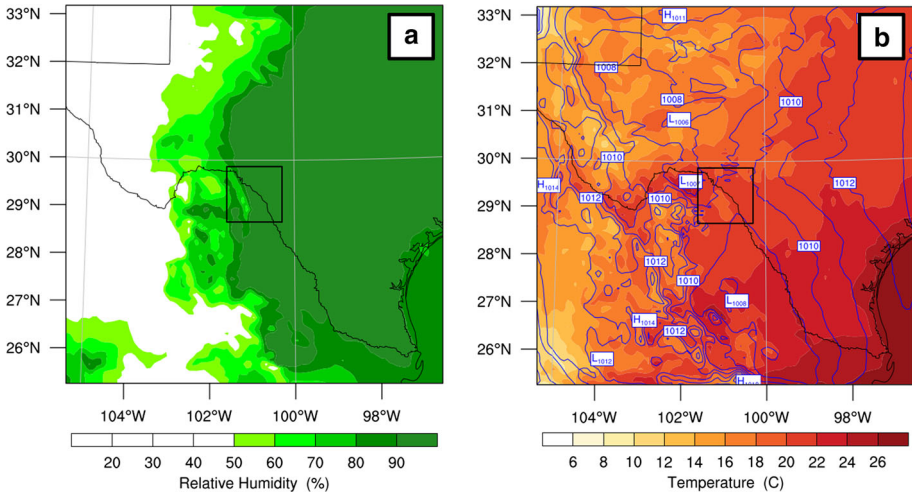


Fig. 8 a Model simulated relative humidity (%) b and temperature (°C) with sea level pressure for domain d1 at 10:50 UTC of May 25, 2015

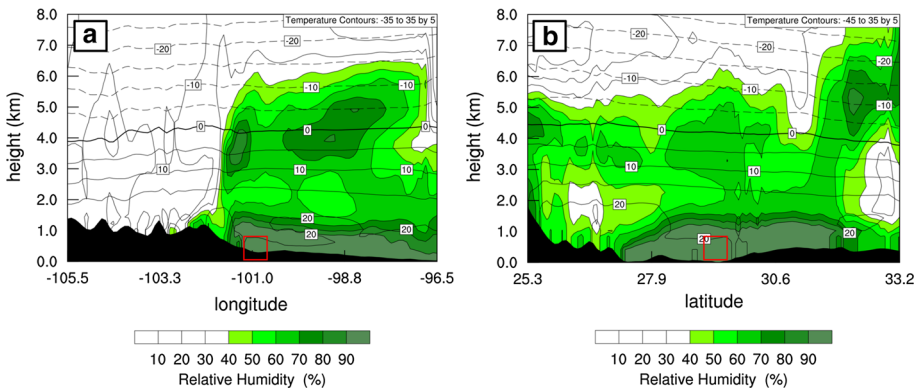


Fig. 9 Vertical cross-section model simulated of temperature (°C) and relative humidity (%) at 10:50 UTC of May 25, 2015

Numerical modeling of extreme atmospheric conditions as supercell storms and tornadoes is very difficult because of two main reasons: (1) The life time of these events are not large enough for being captured in the simulations (spatially and temporally), and (2) the strong gradients and highly variant conditions in atmosphere cannot be represented in the internal physics and parameterizations at mesoscale numerical modeling. Nevertheless, WRF is capable to capture the local meteorological features associated with supercell and severe local storms (Litta et al. 2012). The model results show the relation between horizontal and vertical wind components used for the analysis of convergences and divergences of fluxes and convection zones during the severe storms (Litta et al. 2012). Strong winds regions were located over complex terrain zones, located to the west of Ciudad Acuña, perpendicular at the main direction of the storm motion. These strong winds are northeast oriented, associated with the leading edge of the frontal motion causing a convergent circulation.

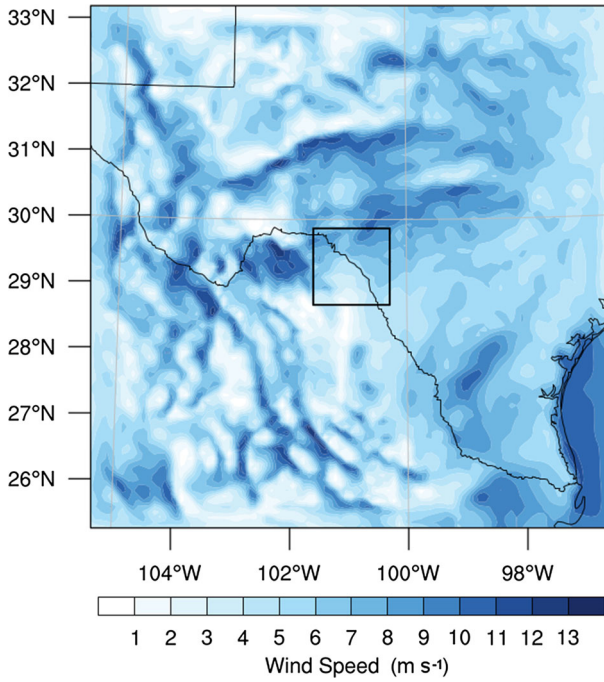


Fig. 10 Model simulated wind speed (m s^{-1}) for domain d1 at 10:50 UTC of May 25, 2015

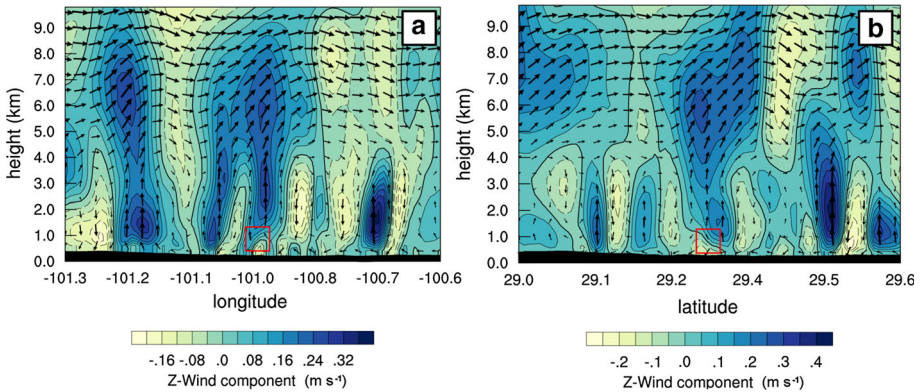


Fig. 11 Vertical cross-section model simulated of Z-wind component (m s^{-1}) and wind vectors at 10:50 UTC of May 25, 2015

As the convergence of the air masses intensified, the formation of the mesocyclone occurred at the 10:50 UTC (very close to the time of tornado occurrence), and the vertical wind shear increased over Ciudad Acuña. In the vertical cross section (E–F), it is possible to observe convective cells formation between heights from 1 to 8 km (Fig. 11a). The wind circulation indicates a typical supercell storms, with downdrafts and updrafts air motion (Fig. 11a, b) (cross sections E–F and G–H). This convergent and divergent circulation indicates the instability in the lower troposphere associated with vertical vorticity acquired

by supercells via the tilting of horizontal vorticity associated with the environmental vertical wind shear (Markowski and Richardson 2009). The distribution of vertical winds also indicates the forced convection.

4.2.3 Absolute vorticity

Absolute vorticity for domain d1 is show in Fig. 12a, anf the values vary from -40×10^{-5} to $80 \times 10^{-5} \text{ s}^{-1}$. There are some areas of positive vorticity extended over the Mexico–USA border with a southeast–northwest direction; and in the southern region areas with positive and negative vorticity, with values of -30×10^{-5} and $70 \times 10^{-5} \text{ s}^{-1}$. The vorticity is associated with updraft and downdraft winds zones (Doswell and Burgess 1993).

However, radar reflectivity is useful for categorizing convective storm, and quantitative analyses by numerical models make it possible to obtain information about storm morphology (Doswell and Burgess 1993). Further, a persistent correlation (positive or negative) between vertical velocity and vertical vorticity is recognized as a practical definition of a supercell (Weisman and Klemp 1984). Figure 12b shows the vertical cross sections (E–F) for domain d3 for absolute vorticity with values ranging from -20×10^{-5} to $60 \times 10^{-5} \text{ s}^{-1}$, which indicates instability in low atmosphere. It is possible to see two areas of positive and negative vorticity near of the surface, although positive vorticity dominates just where the tornado touchdown. The positive values of vorticity are associated with increase in cyclonic circulation and updrafts air motion (Doswell and Burgess 1993; Matsangouras et al. 2016). The rotating updraft winds are widely recognized as characteristic of supercell thunderstorms (Markowski and Richardson 2009). It is also know that vertical vorticity initially arises within thunderstorm updrafts as a result of horizontal vorticity associated with strong vertical wind shear (Doswell and Burgess 1993; Markowski and Richardson 2009).

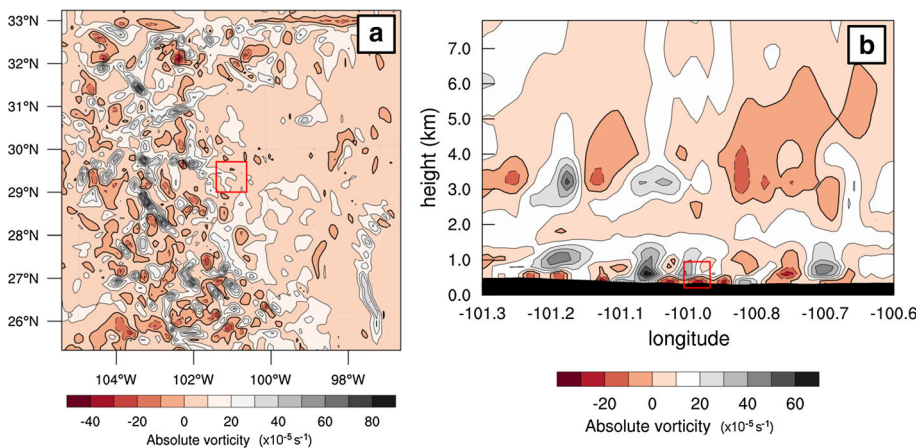


Fig. 12 **a** Absolute vorticity ($\times 10^{-5} \text{ s}^{-1}$) model simulated at 10:50 GMT of May 25, 2015 in mother domain (d1). **b** Vertical cross-section model simulated of absolute vorticity ($\times 10^{-5} \text{ s}^{-1}$) at 10:50 GMT of May 25, 2015, in second nested domain (d3) (**b**)

4.2.4 Storm-relative helicity (SRH) and convective available potential energy (CAPE)

Storm-relative helicity (SRH) is defined as a measure of the potential for cyclonic updraft rotation in right-moving supercells (Davies-Jones et al. 1990). The convective available potential energy (CAPE) represents the amount of buoyant energy available to accelerate a parcel vertically. CAPE indirectly indicates the amount of kinetic energy in an ascending parcel by instability. The SRH and CAPE values are shown in Fig. 13. CAPE positive values represent the vertically integrated positive buoyancy of an adiabatically rising parcel. It is proportional to the amount of kinetic energy that a parcel gains while it is warmer than the surrounding environment. The parcel ascent is enhanced by this instability. CAPE negative values represent the cumulative effect of atmospheric layers that are warmer than the parcel moving vertically along an adiabat. These stable layers often inhibit low-level parcel ascent.

The simulated values of SRH for the low level (0–3 km) for the case of Ciudad Acuña varied between 400 and 500 $\text{m}^2 \text{s}^{-2}$ (Fig. 13b). The areas with higher values ($\sim 600 \text{ m}^2 \text{ s}^{-2}$) were located at the west of the tornado impacted area. The maximum values of SRH were located over the region of Ciudad Acuña in Mexico and Del Rio in USA, which indicate a mesocyclone formation over that area. Other numerical studies for tornadoes analysis reported values of around 100 $\text{m}^2 \text{ s}^{-2}$ (Spain, Mateo et al. 2009) and 289 $\text{m}^2 \text{ s}^{-2}$ in similar tornadic supercell formation (Bangladesh, Bikos et al. 2016).

The simulated CAPE also was calculated for mother domain (Fig. 13b). The highest values of CAPE are extended over the northern region of Ciudad Acuña (Mex) and Del Rio (USA). The values were up of the limit for strong instability ($>2500 \text{ J kg}^{-1}$). CAPE values were of 3000 J kg^{-1} approximately for Ciudad Acuña. Similar results have been reported by Matsangouras et al. (2014a) for three different tornadic cases. There are a relationship between CAPE and relative humidity: cold front interacting with warm moist air is the most important factor for convective potential energy. It has been reported for tornadoes developing in the prefrontal area (cold front activity) (Matsangouras et al. 2014b). Nastos and Matsangouras (2014) showed that almost 48% of tornado events that occurred over the

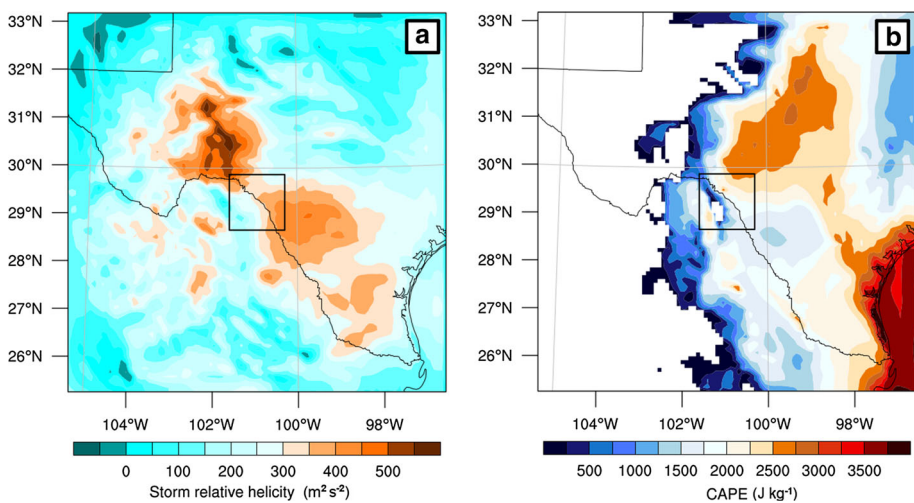


Fig. 13 Storm-relative helicity ($\text{m}^2 \text{ s}^{-2}$) (a) and CAPE (J kg^{-1}) (b) model simulated at 10:50 UTC of May 25, 2015, in domain (d1)

western Greece during the autumn season occurred in prefrontal weather conditions (cold fronts). Once again, SRH and CAPE coincides with those observed in Doppler radar and synoptic charts, in the formation of a supercell storm and great convective activity at the USA–MEX border.

5 Conclusions

The WRF model was able to reproduce mesoscale of atmospheric conditions, before and during the severe tornadic storm. The simulated parameters such as absolute vorticity, CAPE, and SRH indicate the ability of WRF to capture extreme weather events as severe storms. The carried out simulation showed the values of these parameters of the storm with high tornadic potential. This was important since WRF can supplement the very short-term forecast analysis of additional storms to remote sensing. The analyzed event helps us to determine that the frontal activity is an important factor for the tornado genesis early in the tornadic season. The study of climatology on large tornado formation has not included those that occur in southern regions of the tornado alley. In this sense, the tornado analysis of Ciudad Acuña shows how tornadic activity presents a pattern that moves from south to north and intensifies spatially and temporally in the direction to the center of USA. The supercell mechanism not only occurs in conditions of intensifying flows of moisture in summer. It can also be caused as result of high humidity and temperature contrast which are conditioned by late frontal activity and the onset of moisture flux intensifications from the Gulf of Mexico.

References

- Agee E, Jones E (2009) Proposed conceptual taxonomy for proper identification and classification of tornado events. *Weather Forecast* 24(2):609–617
- Akter F, Ishikawa H (2014) Synoptic features and environmental conditions of the tornado outbreak on March 22, 2013 at Brahmanbaria in the east-central region of Bangladesh. *Nat Hazards* 74(3):1309–1326
- Bikos D, Finch J, Case JL (2016) The environment associated with significant tornadoes in Bangladesh. *Atmos Res* 167:183–195
- Bluestein HB (2013) *Severe convective storms and tornadoes*. Springer, Chichester
- Brooks HE, Doswell CA III, Kay MP (2003a) Climatological estimates of local daily tornado probability for the United States. *Weather Forecast* 18(4):626–640
- Brooks HE, Lee JW, Craven JP (2003b) The spatial distribution of severe thunderstorm and tornado environments from global reanalysis data. *Atmos Res* 67:73–94
- Davies-Jones R, Burgess D, Foster M (1990) Test of helicity as a tornado forecast parameter. In: Preprints, 16th conference on severe local storms, Kananaskis Park, American Meteor Society, pp 588–592
- Davies-Jones R, Trapp RJ, Bluestein HB (2001) Tornadoes and tornadic storms. In: *Severe convective storms*. American Meteor Society, pp 167–221
- Doswell CA, Burgess DW (1993) Tornadoes and Tornadic Storms: a review of conceptual models. In: Church C, Burgess D, Doswell C, Davies-Jones R (eds) *The Tornado: its structure, dynamics, prediction, and hazards*. American Geophysical Union, Washington, D. C., pp 161–172
- Dudhia J (1989) Numerical study of convection observed during the winter monsoon experiment using a mesoscale two-dimensional model. *J Atmos Sci* 46(20):3077–3107
- Fuentes OV (2010) The earliest documented tornado in the Americas: Tlatelolco, August 1521. *B Am Meteorol Soc* 91(11):1515
- Fujita TT (1971) *Proposed characterization of tornadoes and hurricanes by area and intensity*. University of Chicago SMRP 91
- Gianfreda F, Miglietta MM, Sansò P (2005) Tornadoes in southern Apulia (Italy). *Nat Hazards* 34(1):71–89

- Goliger AM, Milford RV (1998) A review of worldwide occurrence of tornadoes. *J Wind Eng Ind Aerod* 74:111–121
- Hong SY, Dudhia J, Chen SH (2004) A revised approach to ice microphysical processes for the bulk parameterization of clouds and precipitation. *Mon Weather Rev* 132(1):103–120
- Hong SY, Noh Y, Dudhia J (2006) A new vertical diffusion package with an explicit treatment of entrainment processes. *Mon Weather Rev* 134(9):2318–2341
- Kain JS (2004) The Kain–Fritsch convective parameterization: an update. *J Appl Meteorol* 43(1):170–181
- Litta AJ, Mohanty UC, Prasad SK, Mohapatra M, Tyagi A, Sahu SC (2012) Simulation of tornado over Orissa (India) on March 31, 2009, using WRF–NMM model. *Nat Hazards* 61(3):1219–1242
- Markowski PM, Richardson YP (2009) Tornado genesis: our current understanding, forecasting considerations, and questions to guide future research. *Atmos Res* 93(1):3–10
- Mateo J, Ballart D, Brucet C, Aran M, Bech J (2009) A study of a heavy rainfall event and a tornado outbreak during the passage of a squall line over Catalonia. *Atmos Res* 93(1):131–146
- Matsangouras IT, Nastos PT, Pytharoulis I (2011) Synoptic-mesoscale analysis and numerical modeling of a tornado event on 12 February 2010 in northern Greece. *Adv Sci Res* 6(1):187–194
- Matsangouras IT, Pytharoulis I, Nastos PT (2014a) Numerical modeling and analysis of the effect of complex Greek topography on tornadogenesis. *Nat Hazard Earth Sys* 14(7):1905–1919
- Matsangouras IT, Nastos PT, Bluestein HB, Sioutas MV (2014b) A climatology of tornadic activity over Greece based on historical records. *Int J Climatol* 34(8):2538–2555
- Matsangouras IT, Nastos PT, Pytharoulis I (2016) Study of the tornado event in Greece on March 25, 2009: synoptic analysis and numerical modeling using modified topography. *Atmos Res* 169:566–583
- Medrano MM, García AA (2014) Climatología de tornados en México. *Investigaciones Geográficas, Boletín del Instituto de Geografía* 83:74–87
- Mlawer EJ, Taubman SJ, Brown PD, Lacono MJ, Clough SA (1997) Radiative transfer for inhomogeneous atmospheres: RRTM, a validated correlated-k model for the longwave. *J Geophys Res Atmos* 102(D14):16663–16682
- Nastos PT, Matsangouras IT (2014) Analysis of synoptic conditions for tornadic days over western Greece. *Nat Hazards Earth Syst Sci* 14:2409–2421. doi:10.5194/nhess-14-2409-2014
- National Center for Atmospheric Research (2015) Image archive for 05/25/15. <http://www2.mmm.ucar.edu/imagearchive/>. Accessed 5 Dec 2016
- National Centers for Environmental Information (2015) NEXRAD Data archive for 05/25/15. <https://www.ncdc.noaa.gov/nexradinv/>. Accessed 8 July 2015
- National Centers for Environmental Prediction/National Weather Service/NOAA/U.S. Department of Commerce. 2000, updated daily. NCEP FNL Operational Model Global Tropospheric Analyses, continuing from July 1999. Research Data Archive at the National Center for Atmospheric Research, Computational and Information Systems Laboratory. <http://dx.doi.org/10.5065/D6M043C6>. Accessed 27 May 2015
- Ortiz-Royero JC, Rosales M (2012) Severe tornadoes on the Caribbean coast of Colombia since 2001 and their relation to local climate conditions. *Nat Hazards* 64(2):1805–1821
- Pineda-Martinez LF, Carbajal N (2009) Mesoscale numerical modeling of meteorological events in a strong topographic gradient in the northeastern part of Mexico. *Clim Dyn* 33(2–3):297–312
- Rasmussen EN, Straka JM, Davies-Jones R, Doswell CA III, Carr FH, Eilts MD, MacGorman DR (1994) Verification of the origins of rotation in tornadoes experiment: VORTEX. *B Am Meteorol Soc* 75(6):995–1006
- Ryzhkov AV, Schuur TJ, Burgess DW, Zrníc DS (2005) Polarimetric tornado detection. *J Appl Meteorol* 44(5):557–570
- Servicio Meteorológico Nacional SMN (2015) Redes de Estaciones Meteorológicas Automáticas EMAS. <http://smn1.conagua.gob.mx/emas/>
- Simeonov P, Bocheva L, Gospodinov I (2013) On space–time distribution of tornado events in Bulgaria (1956–2010) with brief analyses of two cases. *Atmos Res* 123:61–70
- Skamarock WC, Klemp JB, Dudhia J, Gill DO, Barker DM, Duda MG, Huang XY, Wang W, Powers JG (2008) A description of the advanced research WRF version 3. NCAR technical note, Mesoscale and Microscale Meteorology Division. National Center for Atmospheric Research, Boulder, Colorado
- Storm Prediction Center (2015) SPC Storm Reports for 05/25/15. <http://www.spc.noaa.gov/climo/reports/>. Accessed 30 May 2016
- Wang W, Barker D, Bray J, Bruyere C, Duda M, Dudhia J et al. (2007) User’s Guide for advanced research WRF (ARW) Modeling System Version 3. Mesoscale and Microscale Meteorology Division–National Center for Atmospheric Research (MMM-NCAR)
- Weisman ML, Klemp JB (1984) The structure and classification of numerically simulated convective storms in directionally varying wind shears. *Mon Weather Rev* 112(12):2479–2498

- Weisz E, Smith N, Smith WL (2015) The use of hyperspectral sounding information to monitor atmospheric tendencies leading to severe local storms. *Earth Space Sci* 2:369–377
- Westbrook C, Clark M (2013) Observations of a tornadic supercell over Oxfordshire using a pair of Doppler radars. *Weather* 68(5):128–134
- Yao Y, Yu X, Zhang Y, Zhou Z, Xie W, Lu Y, Yu J, Wei L (2015) Climate analysis of tornadoes in China. *J Meteorol Res* 29:359–369